General Disclaimer

One or more of the Following Statements may affect this Document

- This document has been reproduced from the best copy furnished by the organizational source. It is being released in the interest of making available as much information as possible.

- This document may contain data, which exceeds the sheet parameters. It was furnished in this condition by the organizational source and is the best copy available.

- This document may contain tone-on-tone or color graphs, charts and/or pictures, which have been reproduced in black and white.

- This document is paginated as submitted by the original source.

- Portions of this document are not fully legible due to the historical nature of some of the material. However, it is the best reproduction available from the original submission.

ON THE REMOTE MEASUREMENT OF EVAPORATION RATES FROM BARE WET SOIL UNDER VARIABLE CLOUD COVER

Siegfried Auer

A & M Associates

8607 Good Luck Road
Lanham, Maryland 20801

Final Report
November 1975 - November 1976

Prepared for

National Aeronautics and Space Administration
Goddard Space Flight Center
Greenbelt, Maryland 20771

TECHNICAL REPORT STANDARD TITLE PAGE

1. Report No.	2. Government Accession No.	3. Recipient's Catalog No.
1		

4. Title and Subtitle	5. Report Date
On the remote measurement of evaporation rates from bare wet soil under variable cloud cover.	November 22, 1976
	6. Performing Organization Code
7. Author(s)	8. Performing Organization Report No.
Siegfried Auer	
9. Performing Organization Name and Address	10. Work Unit No.
A & M Associates 8607 Good Luck Road Lanham, Maryland 20801	11. Contract or Grant No. NAS5-22815
	13. Type of Report and Period Covered Final Report Nov.1975 - Nov. 1976
12. Sponsoring Agency Name and Address National Aeronautics and Space Administration Goddard Space Flight Center	14. Sponsoring Agency Code

15. Supplementary Notes

16. Abstract

Evaporation rates from a natural wet soil surface are calculated from an energy balance equation at 0.1-hour intervals. A procedure is developed for calculating the heat flux through the soil surface from a harmonic analysis of the surface temperature curve. The evaporation integrated over an entire 24-hour period is compared with daily evaporation rates obtained from published models.

17. Key Words (Selected by Author(s))	18. Distribution Statement
Soil Moisture Evaporation Heat Flux	

19. Security Classif. (of this report)	20. Security Classif. (of this page)	21. No. of Pages	22. Price*
Unclassified	Unclassified	37	

*For sale by the Clearinghouse for Federal Scientific and Technical Information, Springfield, Virginia 22151.

Glossary

Symbol	Explanation	Value	Unit
a	albedo of soil for visible and near-infrared light		W cm^{-2}
A	sensible heat warming the air		W cm^{-2}
P	barometric pressure		mbar
c	specific heat		Ws g^{-1} deg^{-1}
D	slope of saturation vapor pressure curve at air temperature		Torr deg^{-1}
e_a, e_d, e_s	saturation vapor pressure at T_a, T_d, T_s		mm Hg = Torr
E	flux of evaporating water		mm day^{-1}
E_a	evaporation term in Penman formula	$0.35\ (e_a-e_d)(1+0.0098u)$	mm day^{-1}
H	net radiation flux		W cm^{-2}
k	thermal conductivity		W cm^{-1} deg^{-1}
L	heat of vaporization of water	2502-2.72t	W s g^{-1}
m	wave number	$\sqrt{\omega/2\kappa}$	cm^{-1}
P	thermal inertia	$\sqrt{k\rho c}$	W $s^{1/2}$ cm^{-2} deg^{-1}
R_a	thermal radiation of atmosphere		W cm^{-2}
R_s	thermal radiation of soil		W cm^{-2}
R_v	visible and near-infrared radiation from sun and sky		W cm^{-2}
S	soil heat flux		W cm^{-2}
t	temperature also: time (in Fourier expression)		deg Celsius
T	temperature		deg Kelvin
T_a, T_d, T_s	temperature of air, dew point, soil surface		deg Kelvin
u	wind speed at approximately 2 meters above the soil surface		m s^{-1} miles day^{-1}
x	soil depth		cm

Glossary (continued)

Symbol	Explanation	Value	Unit
β	Bowen ratio	$\gamma \frac{T_s - T_a}{e_s - e_a} \frac{P}{1000}$	
γ	psychrometric constant (c=specific heat of air, M= molecular weight)	$\frac{c\ P}{L\ M_{H_2O}/M_{air}} = 0.65$	
δ	phase angle of soil heat flux		
ε_s	emissivity of soil for thermal radiation		
$\varkappa$	thermal diffusivity	$\frac{k}{\rho\ c}$	$cm^2\ s^{-1}$
ρ	density		$g\ cm^{-3}$
σ	Stefan-Boltzmann constant	$5.669 \cdot 10^{-12}$	$W\ cm^{-2}\ deg^{-4}$
φ	phase angle		
ω	angular frequency		

ON THE REMOTE MEASUREMENT OF EVAPORATION RATES FROM BARE WET SOIL UNDER VARIABLE CLOUD COVER

1. Introduction

Periodic assessment of soil water content and evaporation rates can greatly benefit agriculture, hydrology, and civil works. Recent research has shown that daily maximum minus minimum surface soil temperature and daily maximum surface soil minus air temperature can be used to estimate soil water content and bare soil evaporation rates (Idso et al, 1975 a, b, c). These procedures have been developed and experimentally verified only for clear-sky conditions. A continuous clear-sky condition is, however, not the normal case, particularly in the eastern US. In an eastern state such as Maryland, it is normal that the sky is at least partly cloud-covered in the afternoon. In order to investigate the feasibility of estimating daily evaporation rates under variable cloud cover, evaporation rates were calculated over 0.1-hour intervals and the results integrated over a 24-hour period. The integrated value agrees reasonably well with calculations in which daily averages of weather parameters were used. The high time resolution provides a vivid history of the evaporation rate during the day and of the condensation rate during the night.

Evaporation from soil under full or near-full cloud cover has not been investigated because of the lack of adequate instrumentation for measuring thermal sky radiation and also because such cloud cover prohibits remote satellite measurements of reflected solar and of thermal radiation from soil, anyway.

2. Experimental Procedure

2.1 Experimental Site

The experiment site was at the Goddard Space Flight Center at Greenbelt, Maryland, at a geographic longitude of $-76^{\circ}51'$ and a geographic latitude of $39^{\circ}\ 0'$. The soil was brought there from a sugar beet field of the Experiment Station of the US Department of Agriculture at Beltsville, Maryland, and had the following composition:

19.6 % clay (particle sizes below 2 μ)
48.9 % silt (particle sizes from 2 to 50 μ)
31.5 % sand (particle sizes greater than 50 μ).

The soil was in a hole 150 cm x 150 cm large and about 25 cm deep. The site was 14 m west of an 8 m high building; thus, the soil surface was in the shadow of the building for about $\frac{\text{arc tan } 8/14}{15 \text{ degrees/hour}} = 2.0$ hours after sunrise and unshadowed thereafter until sunset.

2.2 Temperature Measurements

Eight thermistors were used to obtain air temperatures at 10 and 150 cm above the soil surface and soil temperatures at 0.5, 1, 2, 10 and 20 cm below the soil surface.

Sky radiation temperature in the band from 8 μ to 14 μ was measured occasionally using a thermal radiometer (Barnes Engineering PRT-5). The radiometer had been previously calibrated in the laboratory, using a black body at various known temperatures. Because the radiation temperature of a clear sky was always below the sensitivity range (-20°) of the PRT-5, we covered the aperture with a thin foil. The foil increased the detec-

table thermal radiation by reflecting emitted radiation from the interior of the sensor head back onto the detector and by emitting thermal radiation by itself. The configuration with the foil was calibrated by viewing at cool objects at various temperatures (mostly the sky close to the horizon) and comparing the temperature readings with and without foil.

Two pyranometers were used to measure the total radiation from the hemisphere above the horizon and the reflected radiation from the soil in the visible and near infrared regions of the spectrum. The up-looking pyranometer was placed on top of an instrument rack, 200 cm above the soil surface, whereas the down-looking pyranometer was suspended on a bar, approximately 20 cm above the soil surface. The shadow of the down-looking pyranometer (approximately 0.25 steradian) was usually in its own field of view and as a result the measured albedo was a few percent too low. A correction was made by dividing the pyranometer reading by the solid angle ratio

$$\frac{\pi - 0.25}{\pi} = 0.92$$

2.3 Wind Velocity Measurements

Two cup-anemometers were used to obtain wind velocities at 10 and 150 cm above the soil surface. At wind velocities below 2 m/s, the cups would normally not rotate, and a wind velocity of 1 m/s was assumed.

2.4 Soil Moisture Measurements

Four gypsum block soil moisture sensors were placed in the soil at depths of 2, 5, 10, and 20 cm. Their resistance was measured with alternating current bridges. Temperature readings from thermistors at corresponding

depths were used to correct gypsum block resistance for its temperature dependence.

Core samples were taken from the soil and the volumetric soil moisture was measured gravimetrically in order to calibrate the gypsum block readings.

2.5 Relative Humidity was measured with a sling psychrometer one to four times each day at 10 cm and 150 cm above the ground. Absolute humidity f was computed from relative humidity RH using the formula

$$f = RH \cdot f_{sat} \qquad (1)$$

where f_{sat} is maximum water content of air at temperature T (in ^{o}K),

$$f_{sat}\left[g/m^3\right] \approx 289\,\frac{e}{T} \quad , \qquad (2)$$

e being the saturation water vapor pressure in Torr (or mm Hg)

$$e = \exp\left(-\frac{6735}{T} - 4.819 \ln T + 53.21\right). \qquad (3)$$

It was found that f (at 150 cm only) was usually slowly increasing with time during dry periods and rapidly dropping after a rain. A linear increase of absolute humidity between consecutive readings of relative humidity was, therefore, assumed. Relative humidity between readings was then computed from interpolated absolute humidity values.

2.6 Precipitation was measured using a rain gauge. Qualitative notes were taken on percent cloud cover, haze density and wind type (gusts versus steady wind).

2.7 Data Reduction

All automatic readings were taken at 6 minute intervals on a 24-channel recorder. The readings were manually entered into a Hewlett Packard model

9810 desk calculator which converted the values to physical magnitudes, using laboratory calibration curves. The reduced data were simultaneously printed and plotted. At the same time the calculator performed a harmonic analysis of each curve f (t) over a T = 24-hour period, computing 48 pairs of Fourier coefficients,

$$a_k = \frac{2}{T}\int_0^T f(t)\cos k\omega t\, dt$$

$$\approx \frac{2}{T}\sum_{i=0}^{240} \frac{f(t_{i+1})+f(t_i)}{2}\cos\left(k\omega\frac{t_{i+1}+t_i}{2}\right)(t_{i+1}-t_i) \qquad (4)$$

$$b_k = \frac{2}{T}\int_0^T f(t)\sin k\omega t\, dt$$

$$\approx \frac{2}{T}\sum_{i=0}^{240} \frac{f(t_{i+1})+f(t_i)}{2}\sin\left(k\omega\frac{t_{i+1}+t_i}{2}\right)(t_{i+1}-t_i) \qquad (5)$$

(where $\omega = 2\pi / T$ is the angular frequency and k = 0, 1, 2.....,47 indicates the k-th Fourier coefficient). The a_k, b_k coefficients were converted

$$A_k = \sqrt{a_k^2 + b_k^2} \qquad (6)$$

$$\varphi_k = \arctan\frac{a_k}{b_k} \qquad (7)$$

such that the original curve can be approximated by the sum of its harmonic components as

$$f(t) \approx \frac{a_0}{2} + A_1\sin(\omega t + \varphi_1) + A_2\sin(2\omega t + \varphi_2) + \ldots + A_{47}\sin(47\omega t + \varphi_{47}) \qquad (8)$$

The maximum number of coefficients was given by the number of available storage registers in the calculator.

3. Experimental Results

3.1 Short-wave solar and sky radiation

Figures 1 and 2 show the short-wave radiation R_v on two typically sunny

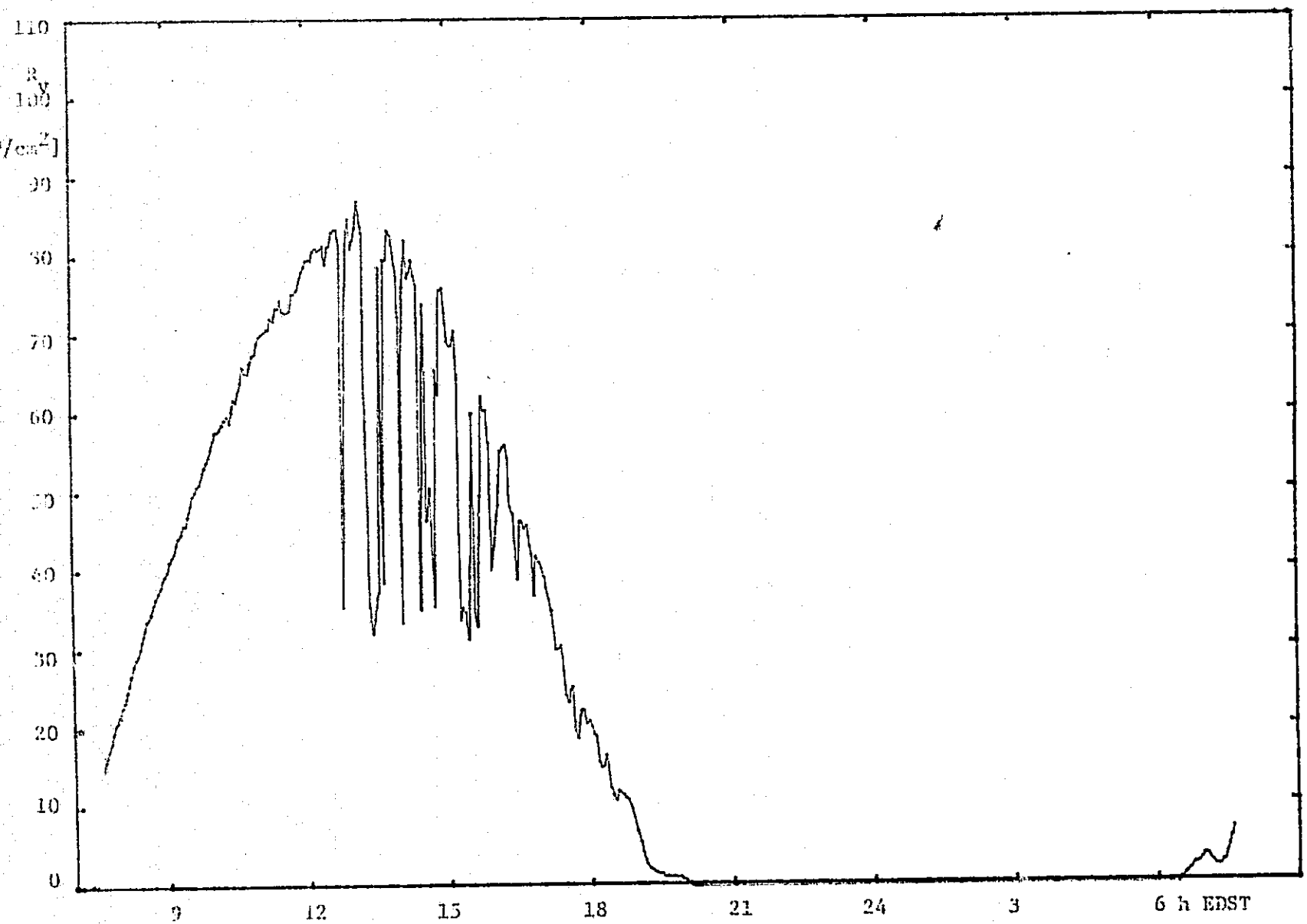

Figure 1. Visible and near-infrared radiation on July 28/29. .

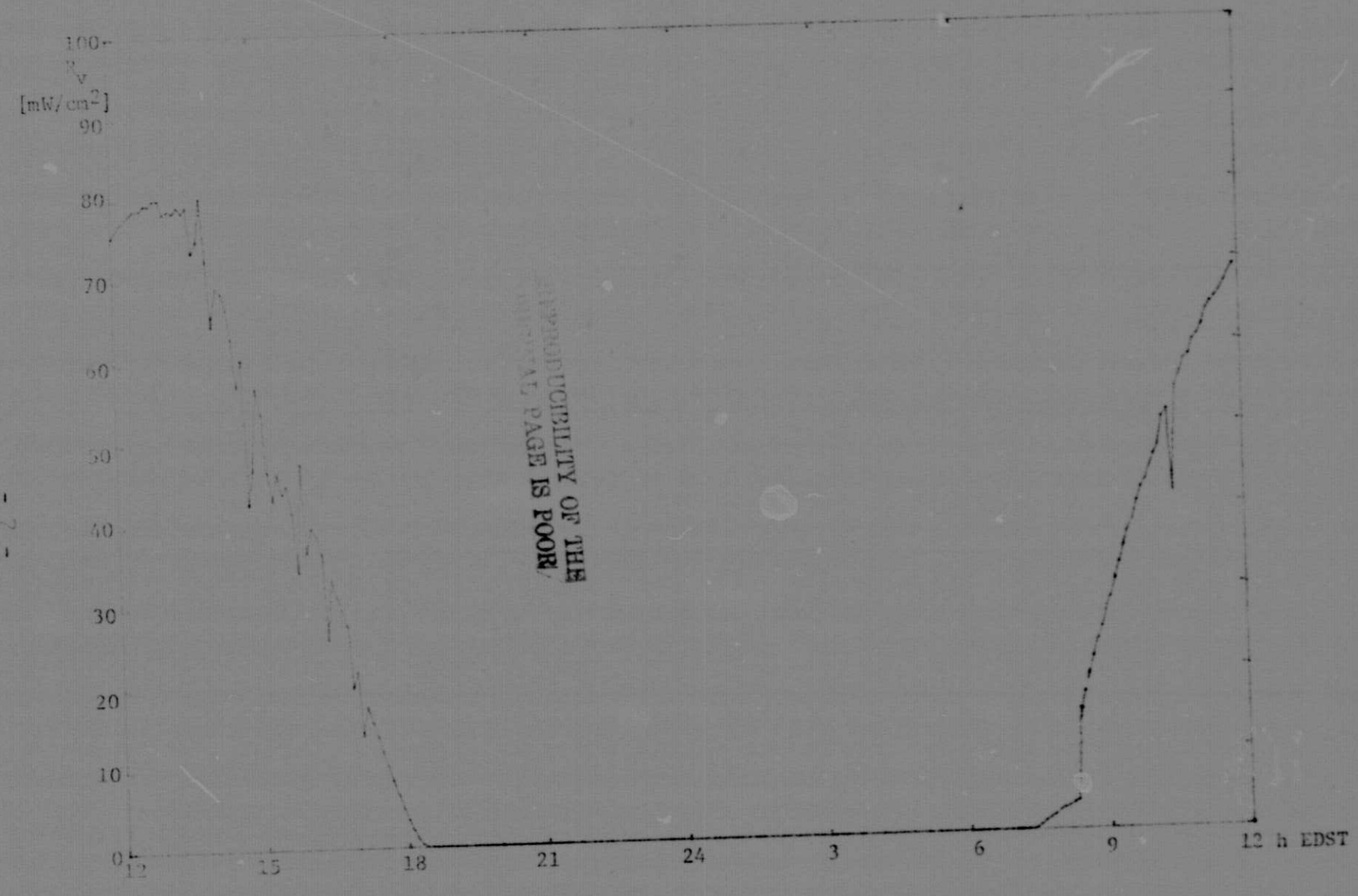

Figure 2. Visible and near-infrared radiation on October 13/14.

days, July 28/29 and October 13/14. Frequent dips in the curves can be noticed, due to increased cloudiness in the afternoon. The reflected radiation is shown in Figure 3 for October 13/14.

3.2 Long-wave sky radiation

The thermal radiation R_a from a clear-sky atmosphere has been calculated from the air temperature T_a [°K] using the semi-empirical Idso-Jackson formula (Idso and Jackson, 1969)

$$R_a [mW/cm^2] \approx \sigma T_a^4 \left\{1 - 0.261 \exp[-0.000777 (T_a - 273)^2]\right\}. \qquad (9)$$

Assuming an emission coefficient for wet soil of $\varepsilon_s = 0.85$, the fraction $0.85\ R_a$ of the thermal sky radiation absorbed by the soil has been calculated for the October 13/14 observation and is shown in Figure 4. It can be seen that this energy flux is nearly constant.

An attempt has been made to measure thermal sky radiation using the PRT-5 radiometer. Figure 5 shows the radiation temperature in the band from 8 to 14 μm as a function of zenith angle on a clear sky (October 22) and on a cloudy sky (October 25). Air temperatures on both days have been between 10 and 15° C. The radiation temperature at zenith angles from 0 to approximately 60 degrees is -35°C for the clear sky and +15° C for the cloudy sky. The corresponding emitted radiation in the band from 8 to 14 μm is 5.4 and 14.3 mW/cm^2, respectively. Although we measured the thermal sky radiation only in the band from 8 to 14 μm, the conclusion appears inevitable that the total radiation from a cloudy sky is significantly higher than that from a clear sky and that the Idso-Jackson formula (9) is not applicable to a cloudy sky.

The best estimate of thermal radiation from a cloudy sky (assuming $\varepsilon = 1$) at an air temperature $T_a = 283$°K is $R_a = 36.4$ mW/cm^2, whereas from a clear

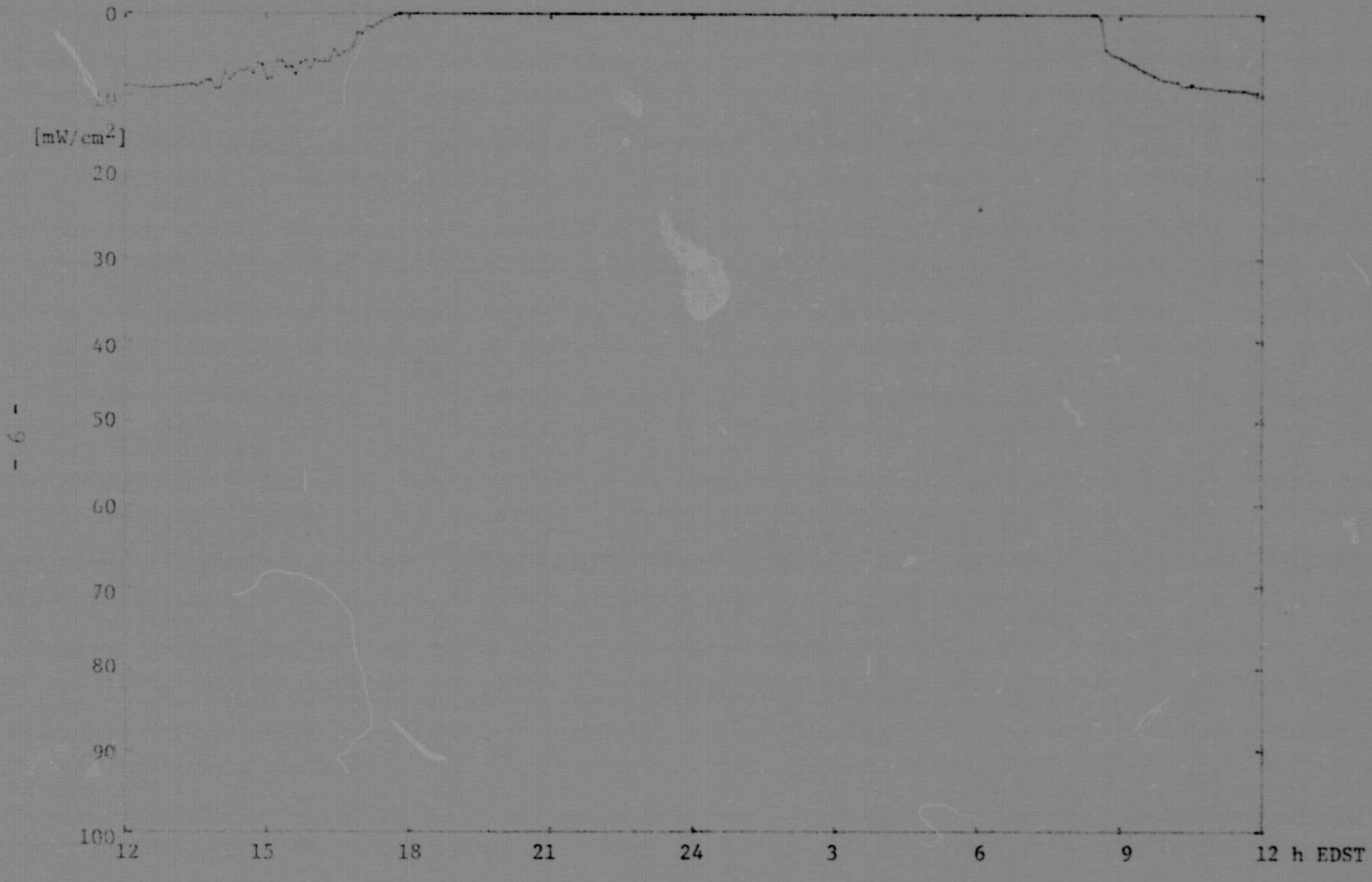

Figure 3. Reflected visible and near-infrared radiation on October 13/14.

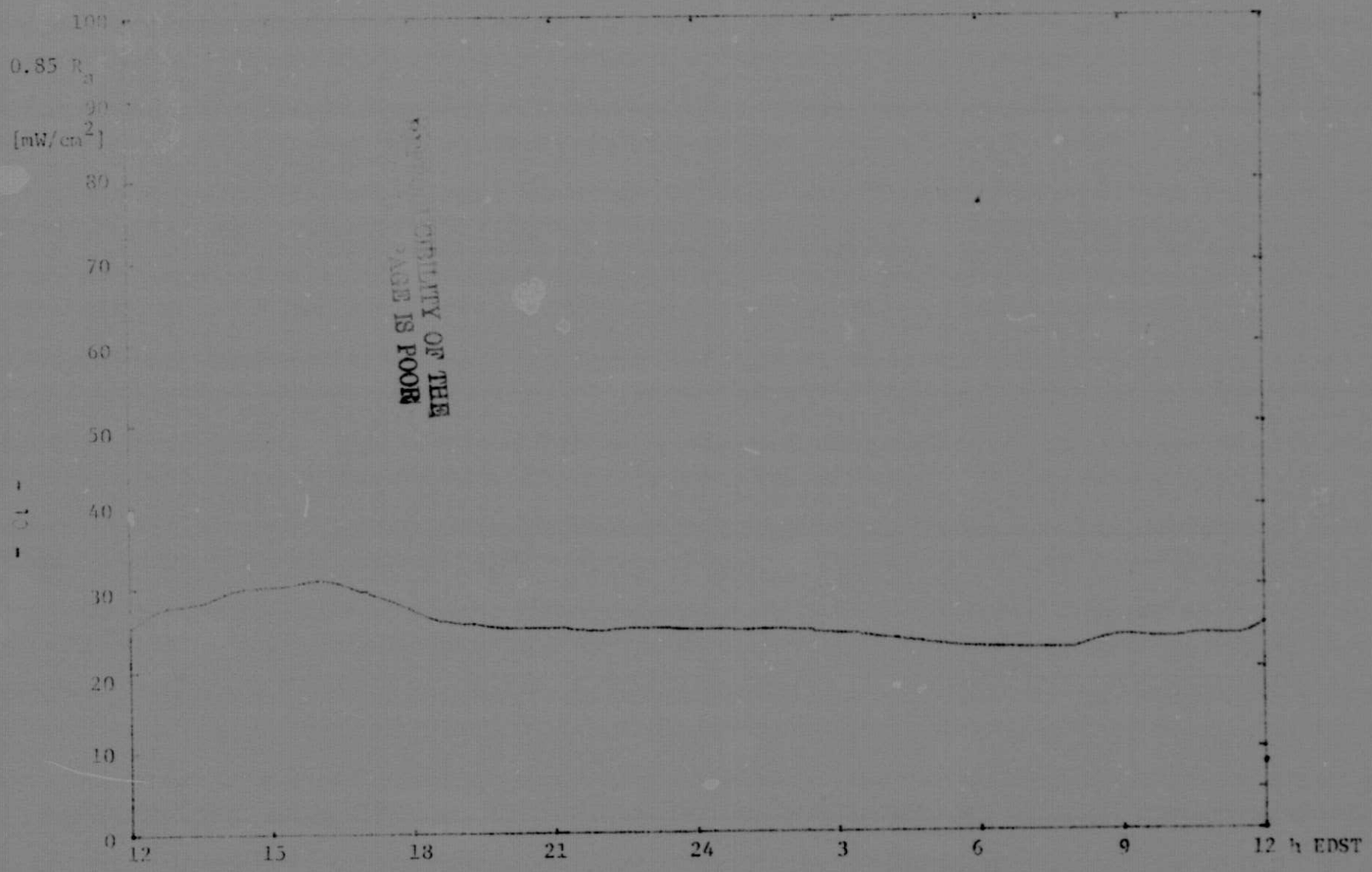

Figure 4. Absorbed thermal sky radiation on October 13/14.

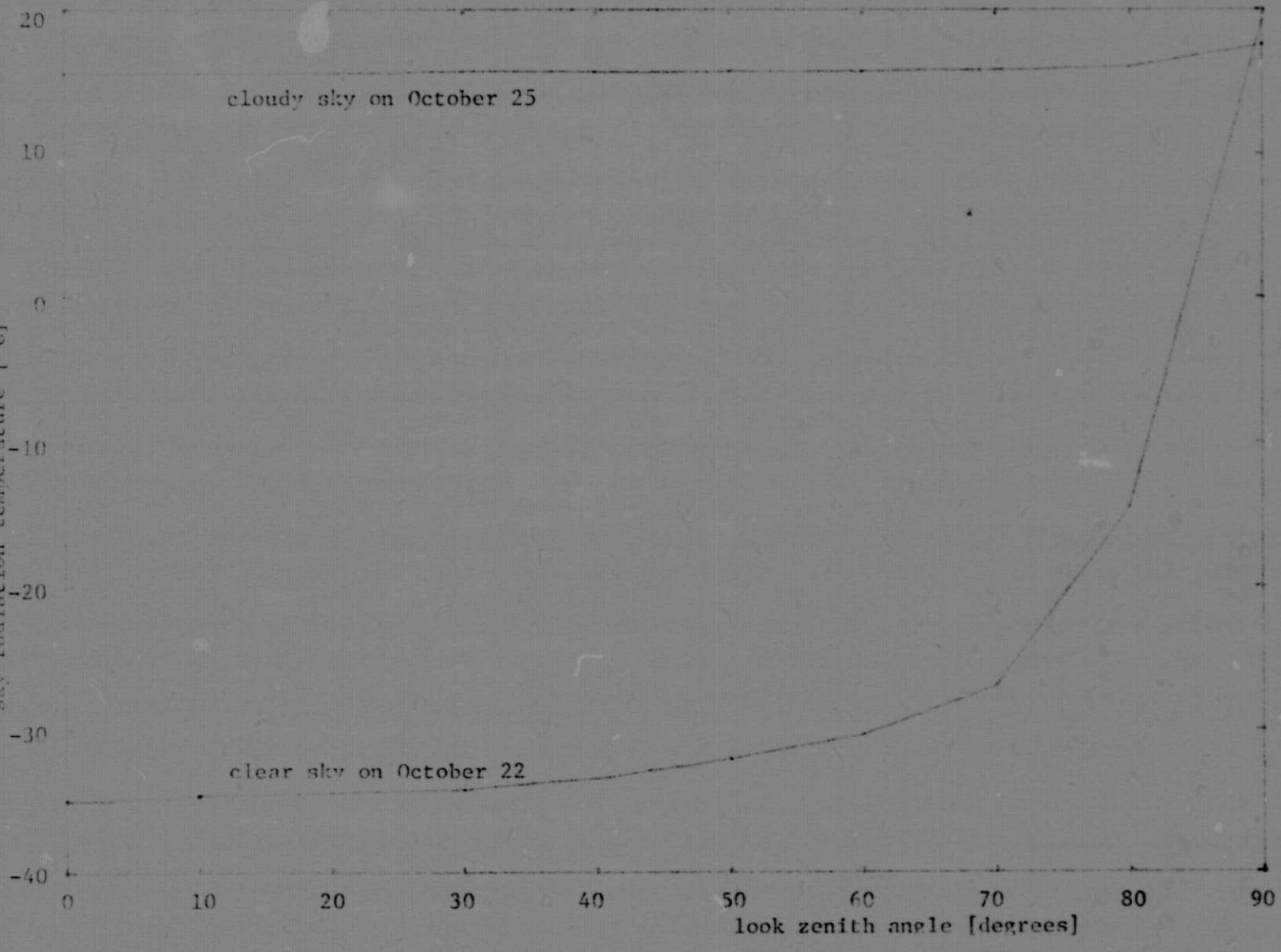

Figure 5. Thermal sky radiation tmperature in the band 8-14 um as a function of look zenith angle.

sky it is R_a = 27.6 mW/cm^2. The difference between those two estimated fluxes, ΔR = 8.8 mW/cm^2, happens to be nearly the same as the difference between the two measured fluxes, ΔR = 8.9 mW/cm^2. This result seems to justify our assumption that the emission coefficient of a dense cloud is nearly unity.

3.3 Long-wave soil radiation

The thermal emission from a soil at temperature T_s [°K] is

$$R_s \left[\text{mW/cm}^2\right] = \varepsilon_s \sigma \; T_s^4 \qquad (10)$$

Assuming again ε_s = 0.85, Figure 6 shows the thermal emission from the soil as calculated for the October 13/14 observation. The energy flux is shown negative because it is directed away from the soil surface.

3.4 Soil Heat Flux

For calculating the heat flux into and out of a soil surface one usually has to know the thermal properties of the soil. Accordingly, an attempt has been made to compute the thermal diffusivity of the soil,

$$\kappa = k/\rho c$$

from the amplitudes and phases of the temperature waves penetrating the soil as given in Table 1. The two approaches used are described by Carslaw and Jaeger (1959)

$$\sqrt{\frac{\omega_i}{2\kappa}} = \frac{\ln T_i(x_1) - \ln T_i(x_2)}{x_2 - x_1} \qquad (11)$$

and

$$\sqrt{\frac{\omega_i}{2\kappa}} = \frac{\varepsilon_i(x_2) - \varepsilon_i(x_1)}{x_2 - x_1} \qquad (12)$$

The temperature curves are shown in Figures 7 – 12 and the Fourier co-

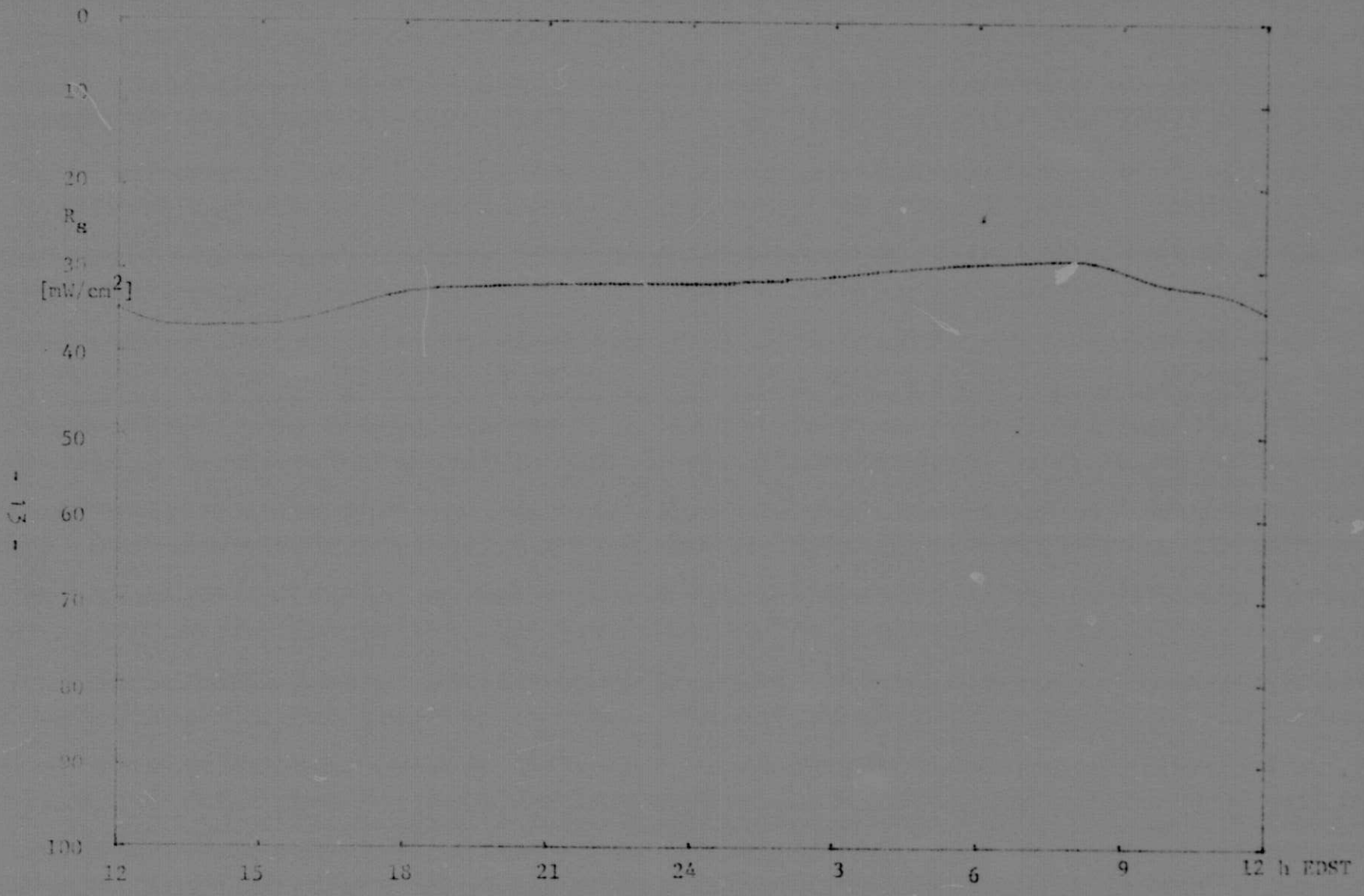

Figure 6. Thermal radiation of soil on October 13/14.

Fourier coefficient→ / phase angle→	A_o	A_1 φ_1	A_2 φ_2	A_3 φ_3	A_4 φ_4	A_5 φ_5	A_6 φ_6	A_7 φ_7	A_8 φ_8	A_9 φ_9	A_{10} φ_{10}	A_{11} φ_{11}	A_{12} φ_{12}	A_{13} φ_{13}	A_{14} φ_{14}	A_{15} φ_{15}	A_{16} φ_{16}
incident light mW/cm^2	19.66	33.3 -103	19.25 64	6.01 -125	0.532 -179	0.492 50	1.64 -14	2.02 158	0.735 -40	0.550 -21	0.751 149	0.357 -16	0.0675 -65	0.391 179	0.519 1	0.300 179	0.040 11
reflected light mW/cm^2	2.68	4.50 -100	2.44 73	0.512 -84	0.719 -160	0.592 21	0.083 -67	0.412 167	0.305 -17	0.042 -58	0.236 142	0.173 -32	0.074 -132	0.117 95	0.06 -42	0.09 -131	0.11 79
soil temperatures degrees Celsius																	
at 0.5 cm	12.50	6.35 -147	4.03 40	0.87 -161	0.165 -83	0.179 43	0.217 -11	0.413 167	0.310 0	0.160 -174	0.134 42	0.149 -134	0.092 -28	0.179 142	0.149 -38	0.160 143	0.138 4
at 1 cm	12.93	5.83 -150	3.51 36	0.73 -156	0.07 -126	0.20 23	0.146 -34	0.31 152	0.24 -13	0.14 178	0.11 28	0.13 -146	0.08 -34	0.13 147	0.11 -37	0.13 132	0.11 -15
at 2 cm	12.72	5.50 -155	3.26 30	0.70 -168	0.09 -85	0.15 22	0.11 -19	0.28 155	0.25 -17	0.14 165	0.09 13	0.09 -147	0.13 -10	0.09 138	0.07 -56	0.07 120	0.09 -4
at 5 cm	12.9	4.41 -168	2.37 11	0.53 162	0.11 -85	0.06 -5	0.07 -1	0.17 154	0.17 -24	0.12 140	0.05 -7	0.05 -149	0.04 19	0.04 135	0.03 -49	0.02 66	0.03 -12
at 10 cm	14.6	2.94 171	1.32 -18	0.285 137	0.057 -88	0.056 -21	0.021 115	0.05 153	0.09 -62	0.06 78	0.02 -100	0.03 -77	0.01 -14	0.01 -120	0.02 -160	0.03 -25	0.01 174
at 20 cm	13.9	1.25 111	0.43 -100	0.19 81	0.19 -109	0.14 24											
soil moisture g/cm^3																	
at 2 cm	0.28	0.06 34	0.03 -162	0.004 39	0.003 -57	0.0004 151											
at 5 cm	0.40	0.05 24	0.03 175	0.007 -86	0.003 -2	0.001 5											
air temperature degrees Celsius																	
at 10 cm	13.2	6.41 -135	4.86 44	1.40 -118	0.43 72	1.16 -129	1.28 41	1.47 -140	1.18 49	1.17 -133	1.10 57	1.05 -142	1.10 41	1.14 -149	1.12 29	0.94 -153	1.05 22
at 150 cm	13.7	5.36 -161	3.14 9	1.12 101	0.79 -109	0.20 172	0.44 -3	0.38 -179	0.06 -1	0.13 -123	0.11 -114	0.15 148	0.22 -24	0.22 -177	0.23 2	0.09 110	0.04 118
wind speed at 150cm m/s	2.40	0.65 -107	0.36 80	0.41 9	0.41 129	0.25 -82	0.14 -167										
heat flux through soil surface mW/cm^2	0	7.58 -102	6.8 85	1.8 -116	0.39 -38	0.48 88	0.63 33	1.3 -148	1.05 45	0.57 -129	0.57 87						
evaporation energy mW/cm^2	8.59	21.4 -112	9.68 21	0.83 169	3.06 168	0.34 -34	2.63 -39	2.97 111	0.27 -19	1.47 -41	0.92 -148	0.75 -17	0.48 -179	1.10 152	1.18 -40	0.70 154	1.03 66
saturation vapor pressure at $T_{0.5}$	11.5	4.93 -14	3.30 35	1.14 176	0.32 -36	0.21 79	0.17 39										
vapor pressure at 150 cm Torr	7.2	2.23 171	0.87 -15	0.40 168	0.28 9	0.26 -171	0.20 4										

Table 1. Fourier coefficients and phase angles of parameters used in this report.

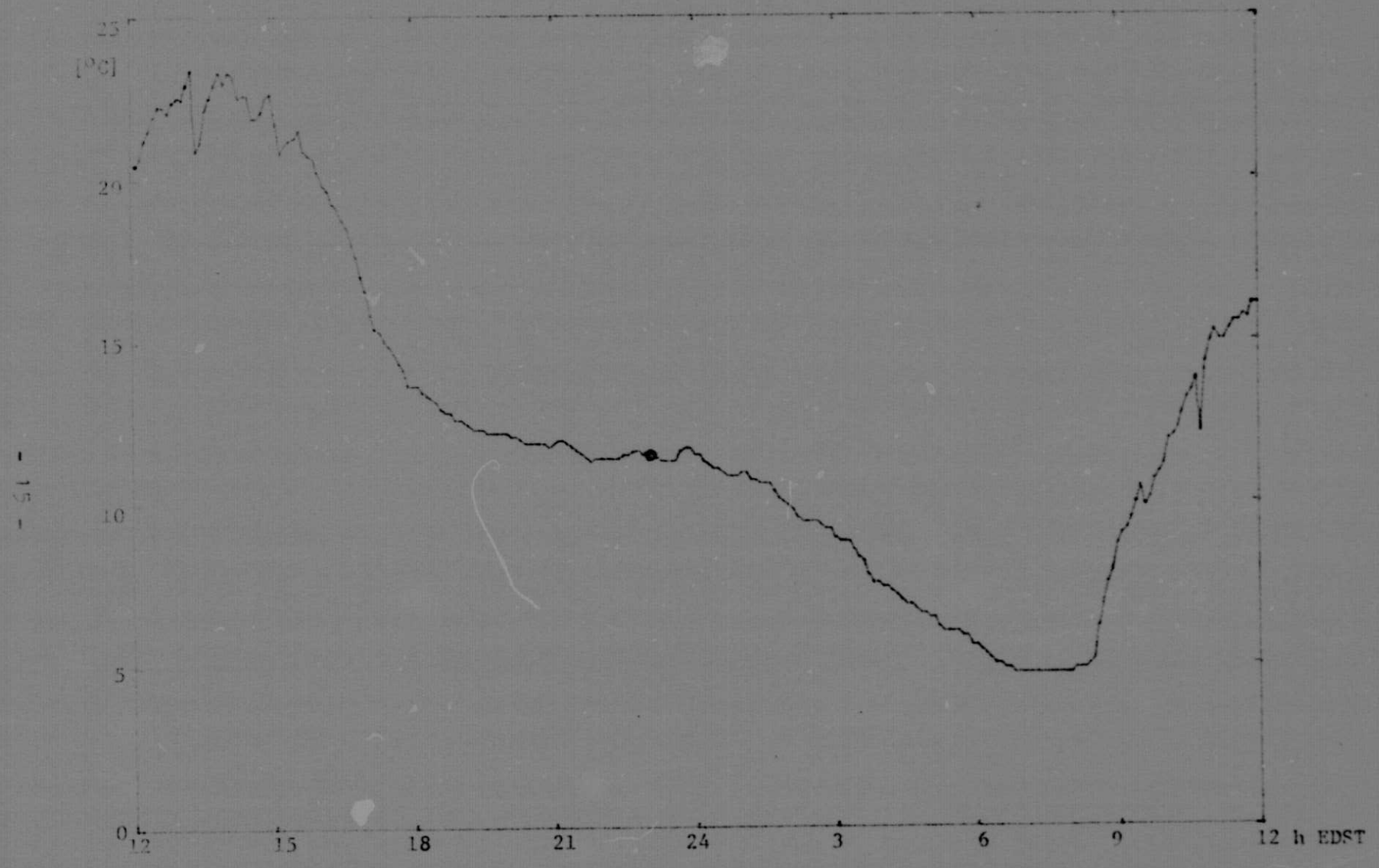

Figure 7. Soil temperature at 0.5 cm on October 13/14.

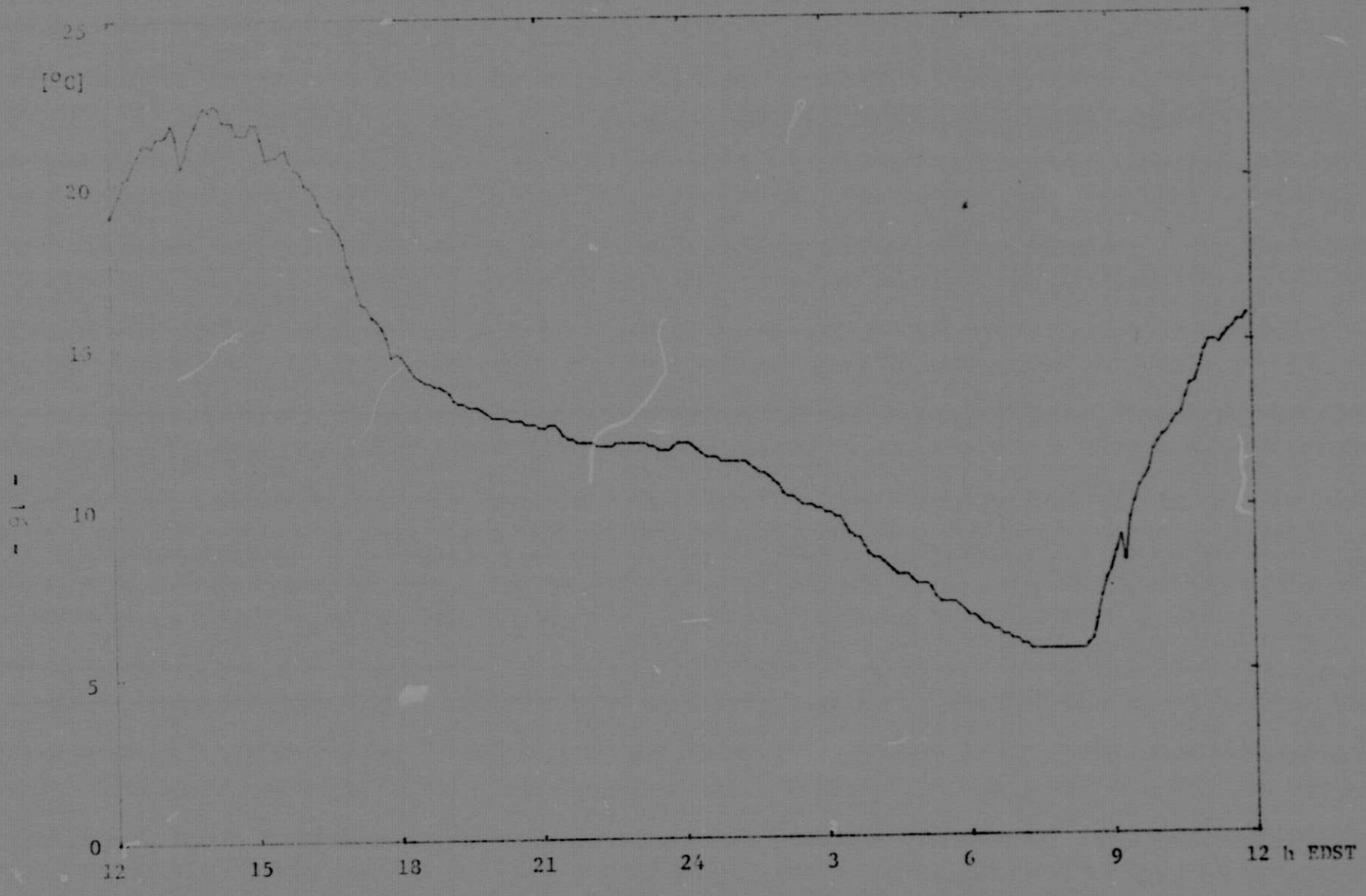

Figure 8. Soil temperature at 1 cm on October 13/14.

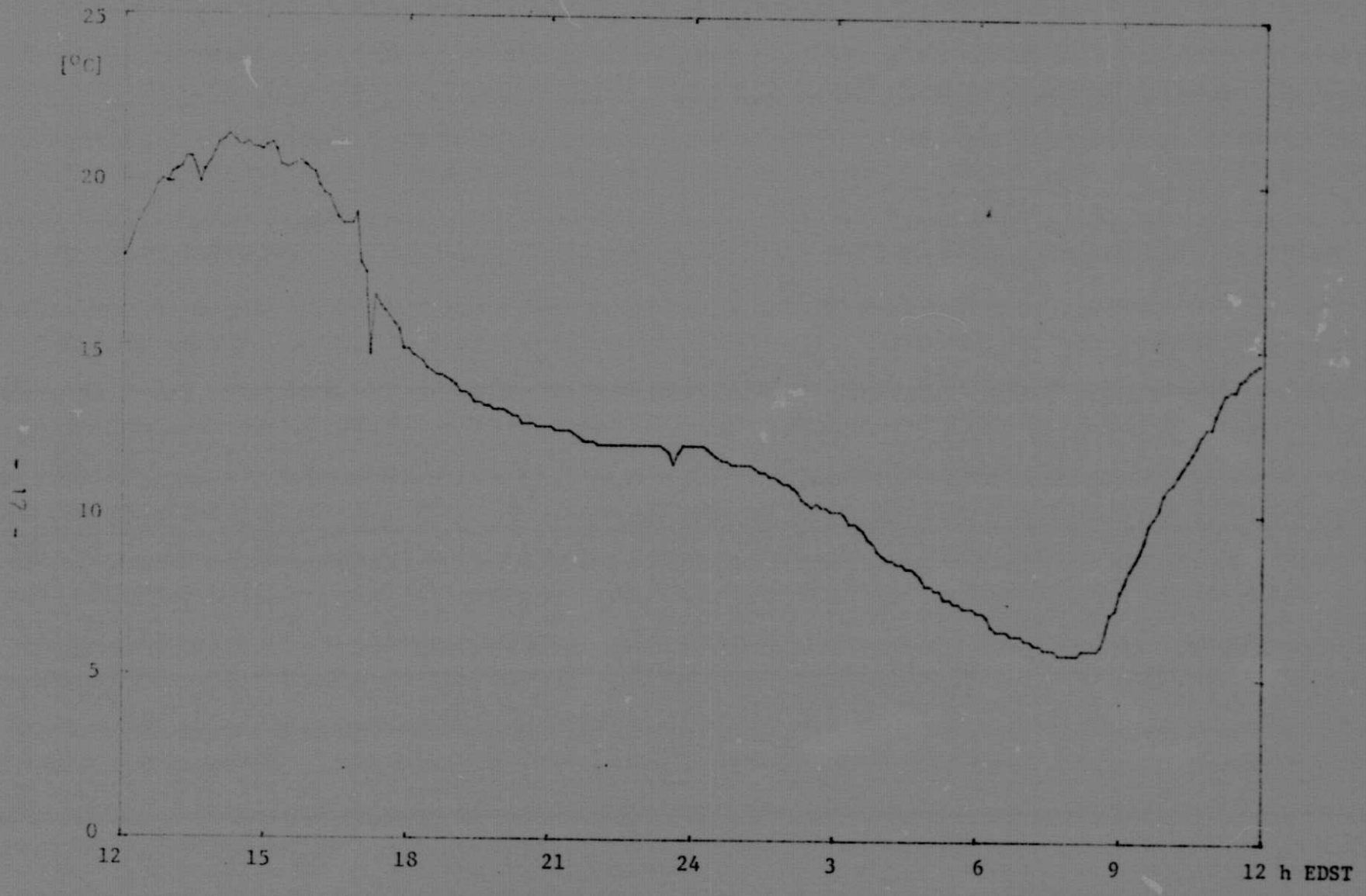

Figure 9. Soil temperature at 2 cm on October 13/14.

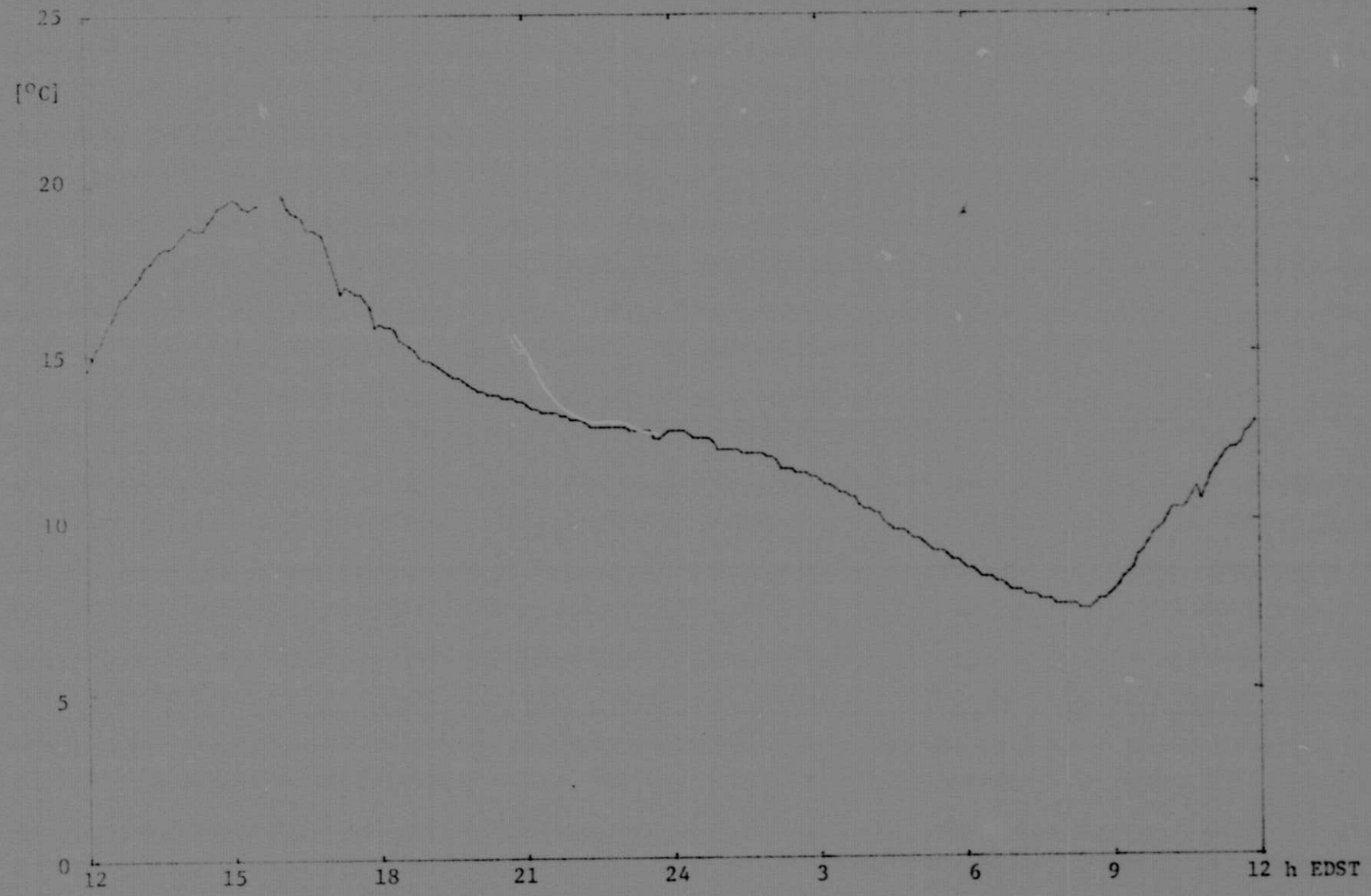

Figure 10. Soil temperature at 5 cm on October 13/14.

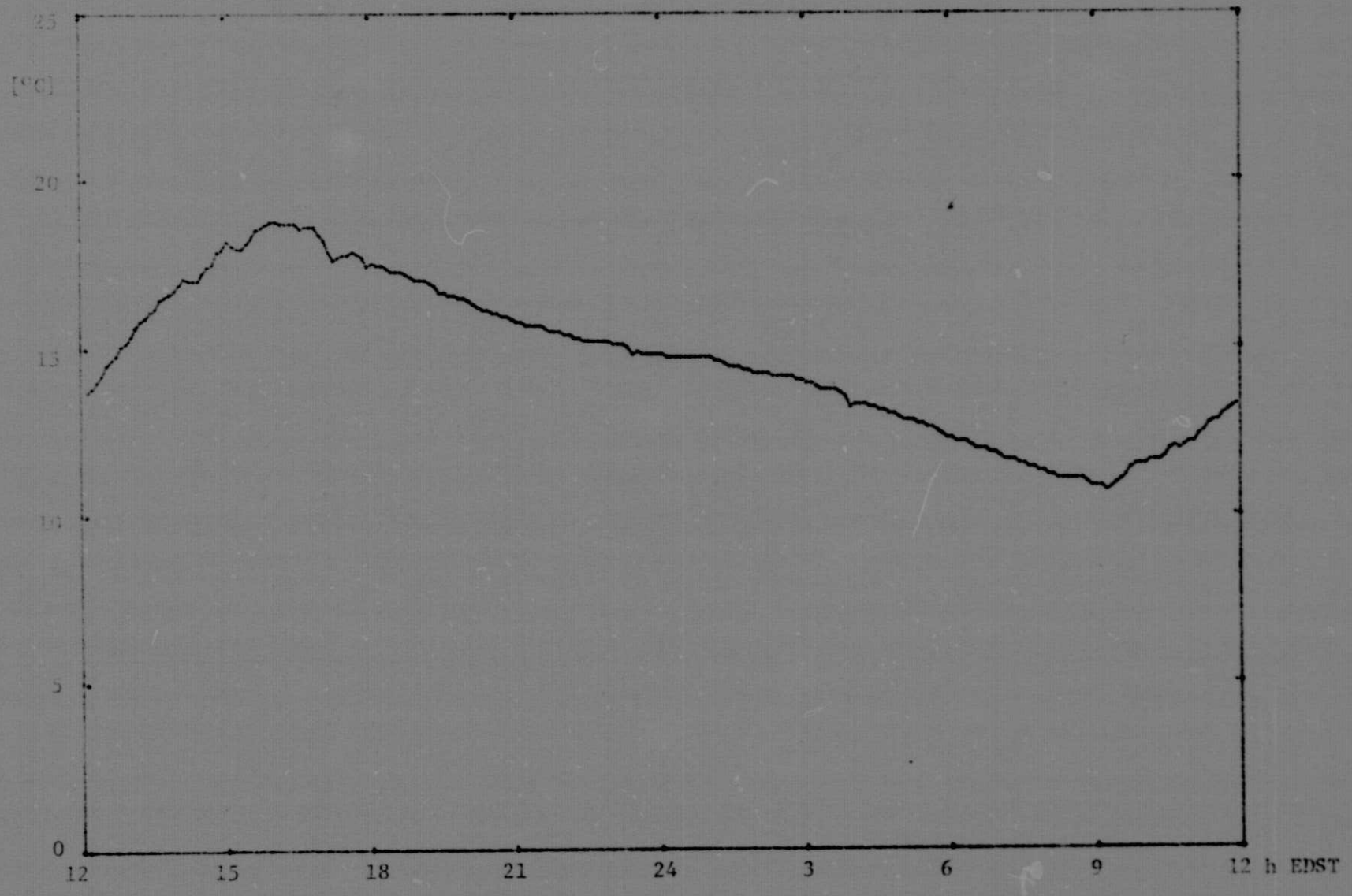

Figure 11. Soil temperature at 10 cm on October 13/14.

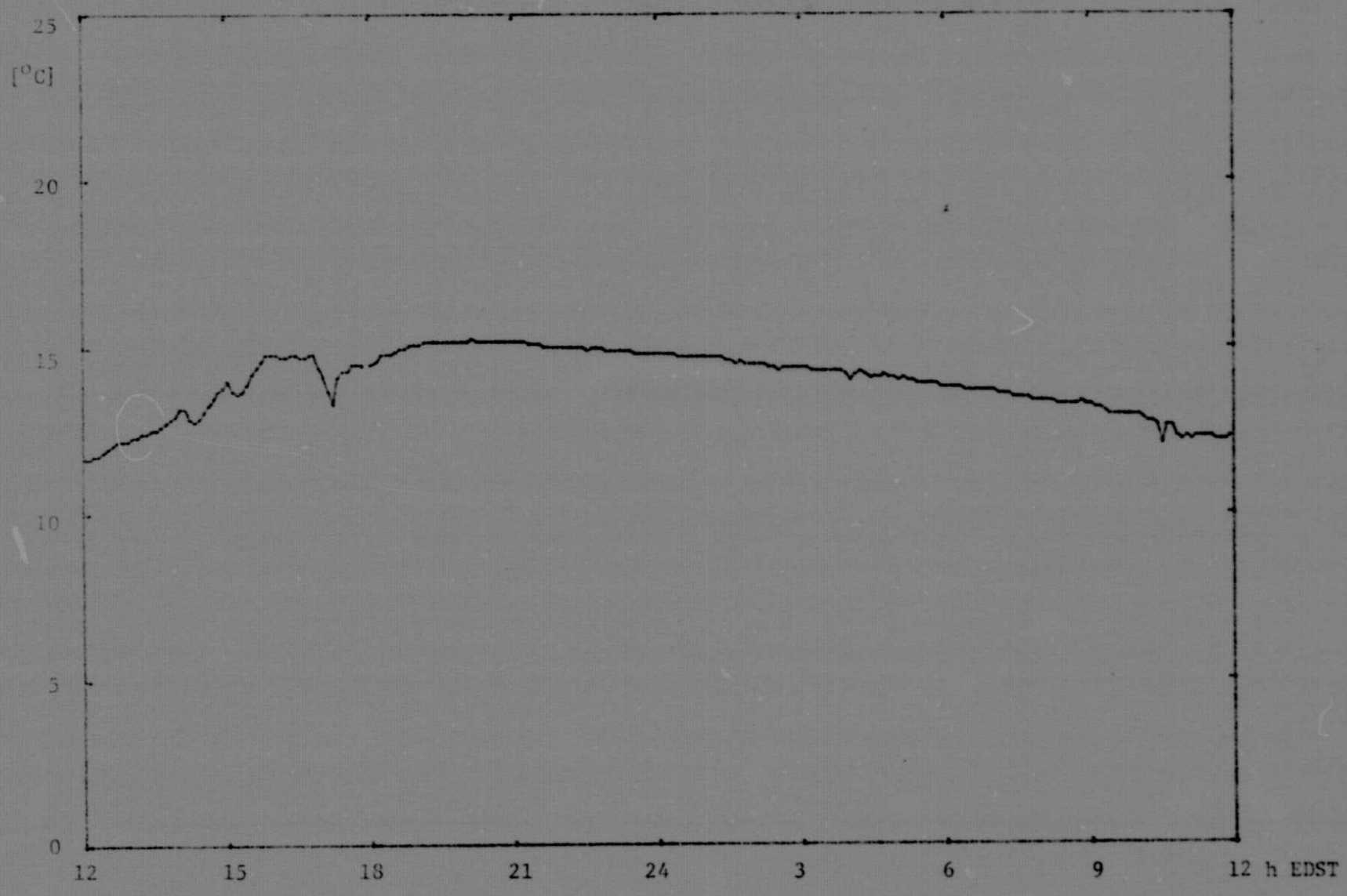

Figure 12. Soil temperature at 20 cm on October 13/14.

efficients of these curves are listed in Table 1. The results are as follows:

layer at depth $x_1 - x_2$	0.5-1 cm	1-2 cm	2-5 cm	5-10 cm	10-20 cm
κ in $cm^2 s^{-1}$					
κ from T_1	0.0012	0.011	0.0067	0.0055	0.0049
T_2	0.00095	0.013	0.0064	0.0053	0.0059
φ_1	0.0033	0.0056	0.0062	0.0070	0.0033
φ_2	0.0039	0.0058	0.0060	0.0072	0.0035
average	0.0023	0.0089	0.0063	0.0063	0.0044

Two characteristics are noticed. First, the thermal diffusivity of the layer from 0.5 to 1 cm is significantly lower than at layers below 1 cm. This is interpreted as an indication of a lower soil moisture content near the soil surface. Second, although the values calculated from T_1 agree well with those calculated from T_2, and the values calculated from φ_1 agree well with those calculated from φ_2, the two approaches lead to significantly different results. While in the uppermost layer $\kappa(T)$ equals only about $0.3\kappa(\varphi)$, in the next deeper layer the situation is reversed and $\kappa(T) \approx 2\ \kappa(\varphi)$.

It is believed that the disagreement is caused by an energy transport mechanism different from heat conduction, such as diffusion of water or water vapor through the soil, and that the procedures assuming heat conduction as the only transport mechanism are not directly applicable to a wet soil.

A different approach starts from the assumption that the thermal inertia is known. Since the thermal inertia of an average moist soil is P = 0.14 and that of water P = 0.16, our assumption appears to be justified. The

heat flux is calculated using only the curve of the temperature at the soil surface.

When the soil temperature T at a depth x is a periodic function of time of period $2\pi/\omega$ = 24 hours,

$$T = T_0 + \sum_{i=1}^{\infty} T_i \exp(-m\sqrt{i}\,x)\sin(i\omega t - m\sqrt{i}\,x + \varphi_i) \qquad (13)$$

(where $m = \sqrt{\frac{\omega}{2\kappa}}$ is the wave number of a temperature wave whose wavelength is $\lambda = \frac{2\pi}{m}$, κ being the thermal diffusivity of the material, $\kappa = \frac{k}{\rho c}$) then the flux of heat into the soil is

$$S = -k\frac{\partial T}{\partial x} \qquad (14)$$

$$S = k m \sum_{i=1}^{\infty} T_i \sqrt{i}\, e^{-m\sqrt{i}\,x}\left[\sin(i\omega t - m\sqrt{i}\,x + \varphi_i) + \cos(i\omega t - m\sqrt{i}\,x + \varphi_i)\right] \qquad (15)$$

We may use the identity

$$\sin\alpha + \cos\alpha \equiv \sqrt{2}\sin\alpha\cos 45^\circ + \sqrt{2}\cos\alpha\sin 45^\circ \equiv \sqrt{2}\sin(\alpha + 45^\circ) \qquad (16)$$

to obtain

$$S = k m \sqrt{2} \sum_{i=1}^{\infty} T_i \sqrt{i}\, e^{-m\sqrt{i}\,x}\sin(i\omega t - m\sqrt{i}\,x + \varphi_i + 45^\circ) \qquad (17)$$

At the surface, x = 0, we have

$$T_{surface} = T_0 + \sum_{i=1}^{\infty} T_i \sin(i\omega t + \varphi_i) \qquad (18)$$

$$S_{surface} = k m \sqrt{2} \sum_{i=1}^{\infty} T_i \sqrt{i}\sin(i\omega t + \varphi_i + 45^\circ) \qquad (19)$$

Substituting

$$\sqrt{2}\,k m = k\sqrt{\frac{\omega}{\kappa}} = \sqrt{\omega}\sqrt{k\rho c} = \sqrt{\omega}\,P \qquad (20)$$

P being the thermal inertia of the soil, we obtain

$$S_{surface} = \sqrt{\omega}\, P T_1 \sin(\omega t + \varphi_1 + 45°) + \sqrt{2\omega}\, P T_2 \sin(2\omega t + \varphi_2 + 45°) + \ldots \quad (21)$$

$$= S_1 \sin(\omega t + \delta_1) + S_2 \sin(2\omega t + \delta_2) + \ldots \quad (22)$$

We see that the transformation from the Fourier coefficients of the temperature curve T_i, φ_i to those of flux curve S_i, δ_i follows the rules

for the ith amplitude $$S_i = \sqrt{i\omega}\, P T_i \quad (23)$$

and for the ith phase $$\delta_i = \varphi_i + 45° \quad (24)$$

Figure 7 shows the soil surface temperature T_s on October 13/14. A harmonic analysis results in the following expression:

$$T[°C] = 12.5 + 6.35 \sin(\omega t - 147.2°) + 4.03 \sin(2\omega t + 40.4°) + \ldots\ldots \quad (25)$$

Assuming a thermal inertia typical for wet soil,

$$P = 0.14\ W_s^{1/2}\ cm^{-2}\ °K^{-1}$$

the heat flux into the soil surface can now be calculated, following equations (23) and (24)

$$S[mW/cm^2] = 7.58 \sin(\omega t - 102.2°) + 6.8 \sin(2\omega t + 85.4°) + \ldots. \quad (26)$$

The first 16 pairs of Fourier coefficients of both T and S curves are listed in Table 1. S is shown in Figure 13.

3.5 Heat of Evaporation and Sensible Heat

The sum of all energy fluxes must be zero,

$$R_v (1-a) + \varepsilon_s R_a - \varepsilon_s R_s - S - \rho L E - A = 0 \quad (27)$$

$\rho L E$ is the evaporation energy and A is the sensible heat used to warm the air. Using Bowen's ratio $\beta = \frac{A}{\rho L E}$, and rearranging eq. (27) gives

$$E = \frac{R_v (1-a) + \varepsilon_s (R_a - R_s) - S}{\rho L (1+\beta)} \quad (28)$$

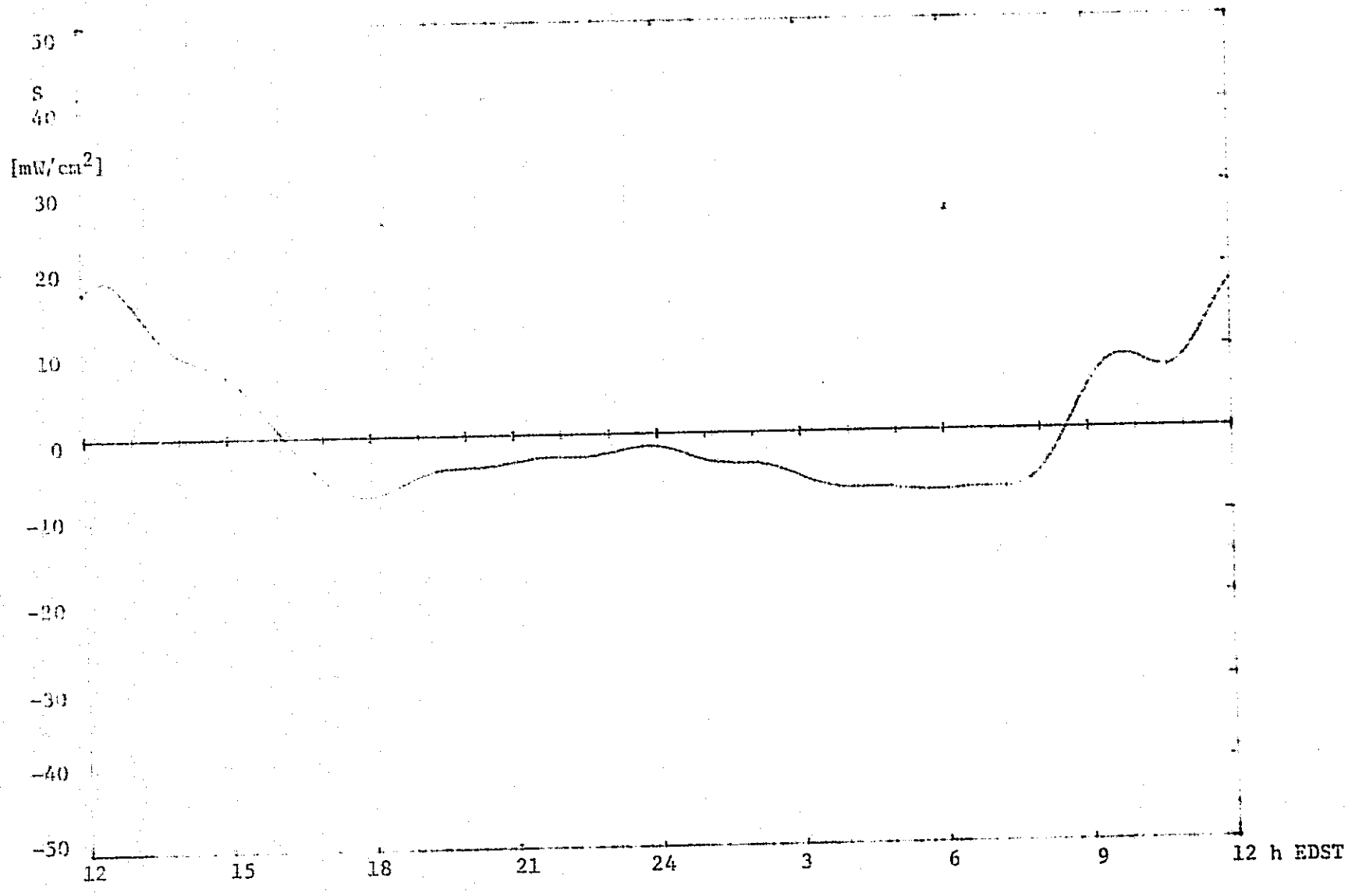

Figure 13. Calculated heat flux through the soil surface.

The Bowen ratio is plotted in Figure 14 for the October 14/14 observation. The result of a point-by-point calculation of E is shown in Figure 15. The energy available for evaporation can be expressed by

$$\rho LE = 8.59 + 21.4 \sin(\omega t - 112.4°) + 9.7 \sin(2\omega t + 21.5°) + \ldots \quad [mW/cm^2] \qquad (29)$$

The evaporation becomes negative during the night, indicating condensation of water on the soil surface. The integrated flux of evaporating water during the 24-hour period is calculated from the first coefficient of eq. (29),

$$E = \frac{8.59\ mW/cm^2 \cdot 86400\ s}{1\ g/cm^3 \cdot 2.47 \cdot 10^6\ mWs/g} = 0.3\ cm/day = 3\ mm/d$$

3.6 Summary of Energy Fluxes

The contributions of the various kinds of energy, averaged over 24 hours are summarized below (all in mW/cm^2)

incident light	19.7
reflected light	- 2.7
thermal soil radiation	- 27.3
thermal sky radiation absorbed by soil	25.2
heat flux through soil surface	0
evaporation energy	- 8.6
sensible heat to warm air (balance)	- 6.3

The dominant contribution of thermal radiation from both soil and sky should be noticed. A poor estimate can lead to a large error in the calculated evaporation rate.

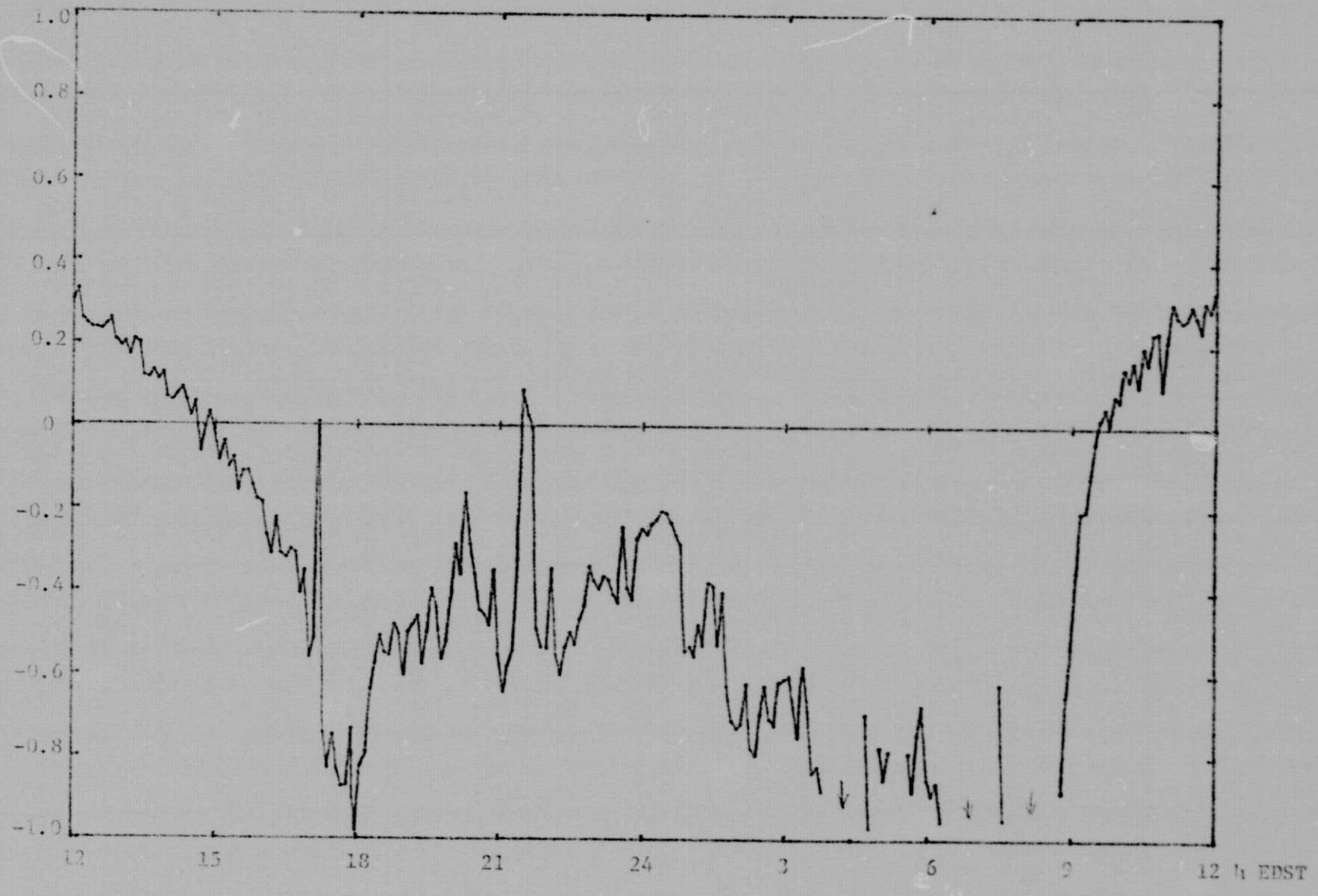

Figure 14. Bowen ratio, October 13/14.

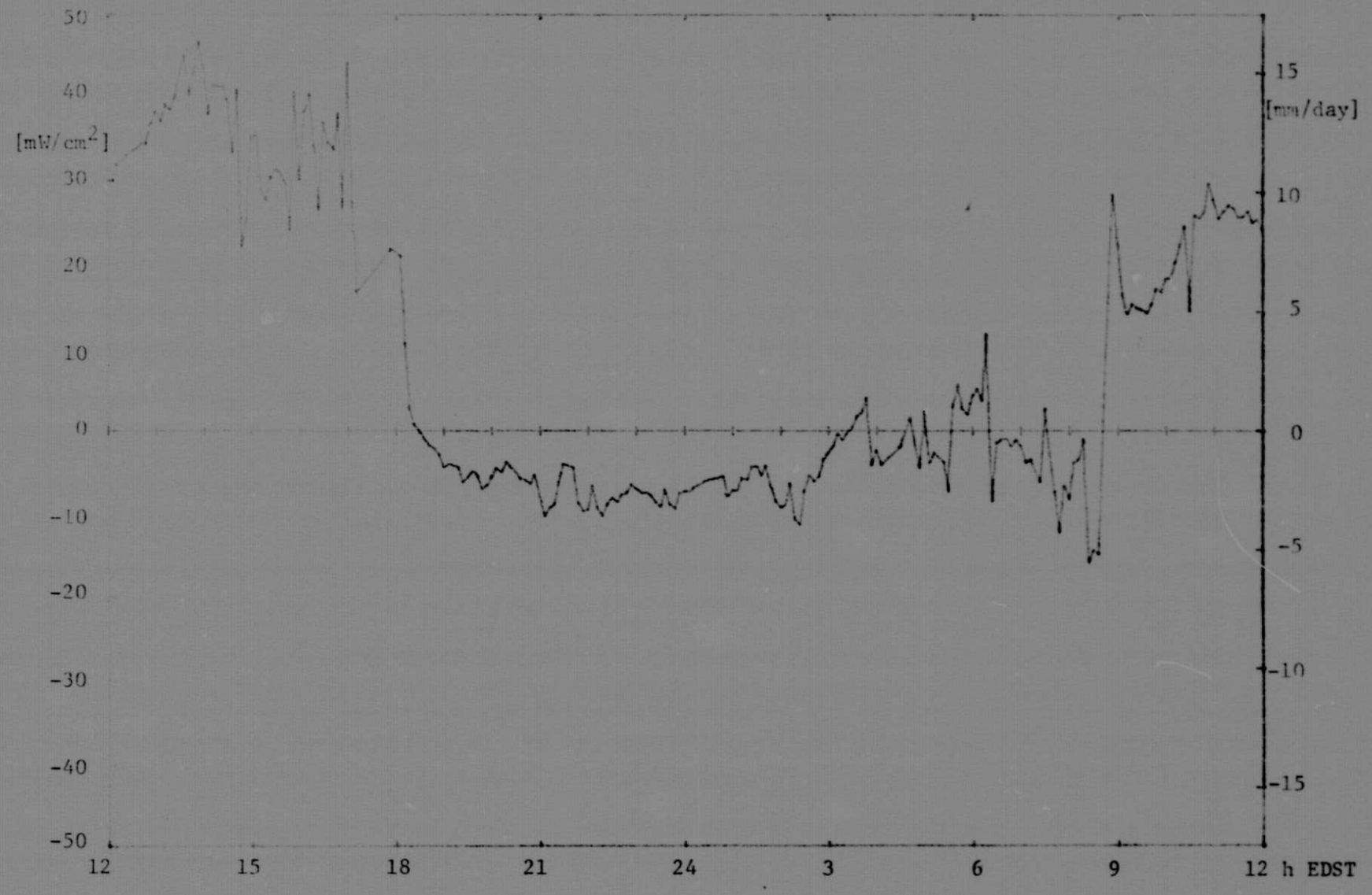

Figure 15. Heat of evaporation (left-hand scale) and rate of evaporation (right-hand scale) on October 13/14.

4. Comparison of Calculated Evaporation with Published Models

Using as the daily average of a weather parameter its 0-th Fourier coefficients as given in Table 1, we may calculate daily evaporation rates from published models and compare the results with our 24-hour evaporation flux.

4.1 Sink Strength Approaches

Rohwer (1931) found empirically

$$E = 0.40\ (e_s - e_d)\ (1 + 0.0071\ u) \qquad (30)$$

Wind speed u (miles per hour) on October 13/14 at 0.1 m and 1.5 m is shown in Figures 16 and 17, respectively. Using the average wind speed at 1.5 m, u = 2.4 m/s, we obtain

$$E = 3.3 \text{ mm/d.}$$

Four formulae given by Penman (1948) yield the following results:

$$E = 0.065\ (e_s - e_d)\ u^{0.54} = 3.9 \text{ mm/d,} \qquad (31)$$

$$E = 0.033\ (e_s - e_d)\ u^{0.68} = 3.9 \text{ mm/d,} \qquad (32)$$

$$E = 0.30\ (1 + 0.0142\ u)\ (e_s - e_d) = 3.7 \text{ mm/d,} \qquad (33)$$

$$\text{and } E = 0.35\ (1 + 0.0098\ u)\ (e_s - e_d) = 3.4 \text{ mm/d.} \qquad (34)$$

Penman considers the last equation to be the best form.

4.2 Energy Balance Approaches

The Penman (1948) formula for an energy balance approach gives

$$E = \frac{\Delta H + E_a \gamma}{\Delta + \gamma} = 3.8 \text{ mm/d.} \qquad (35)$$

Using a formula of Bertholic et al. for potential evaporation from a wet surface,

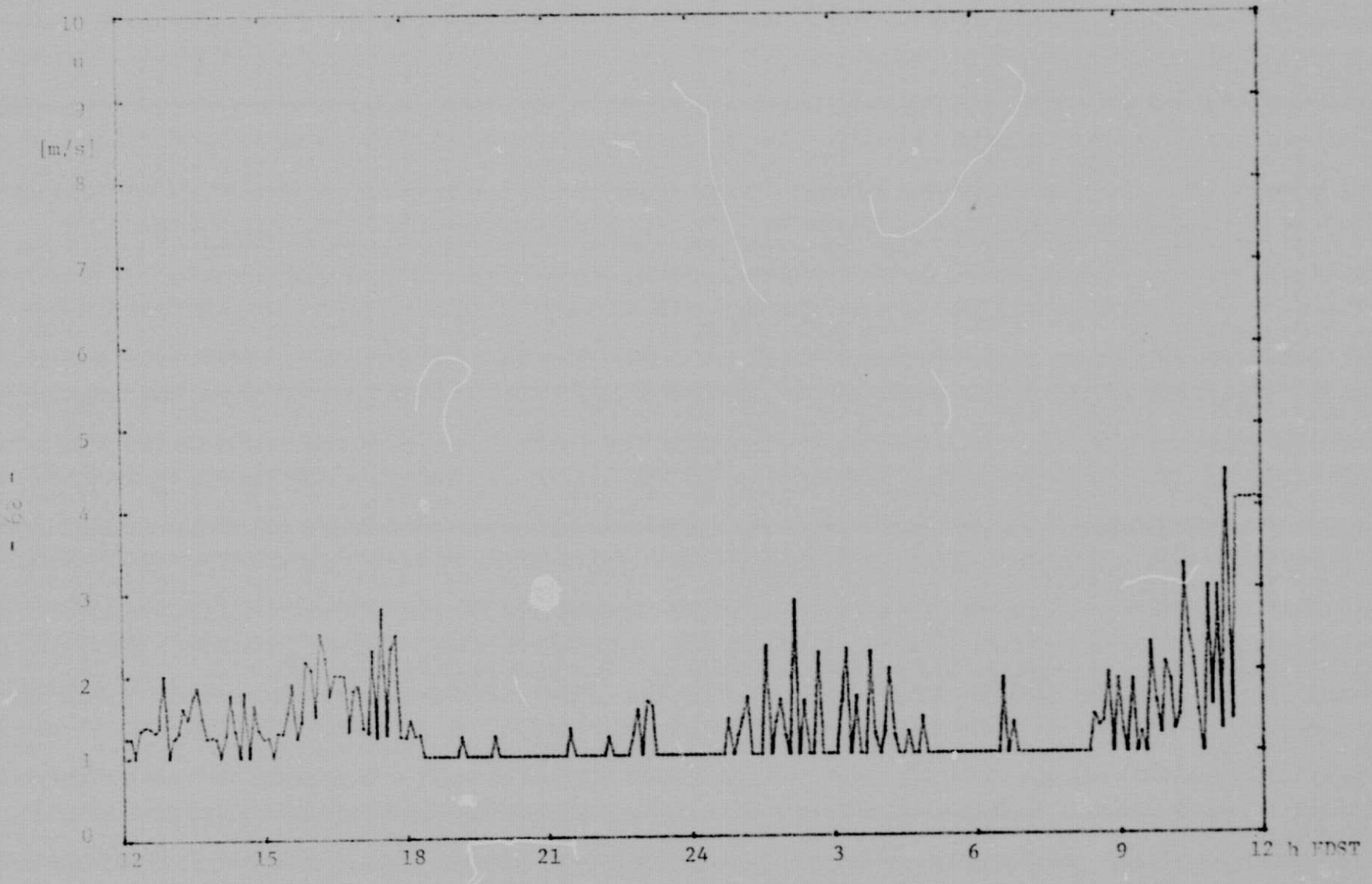

Figure 16. Wind speed at 10 cm on October 13/14.

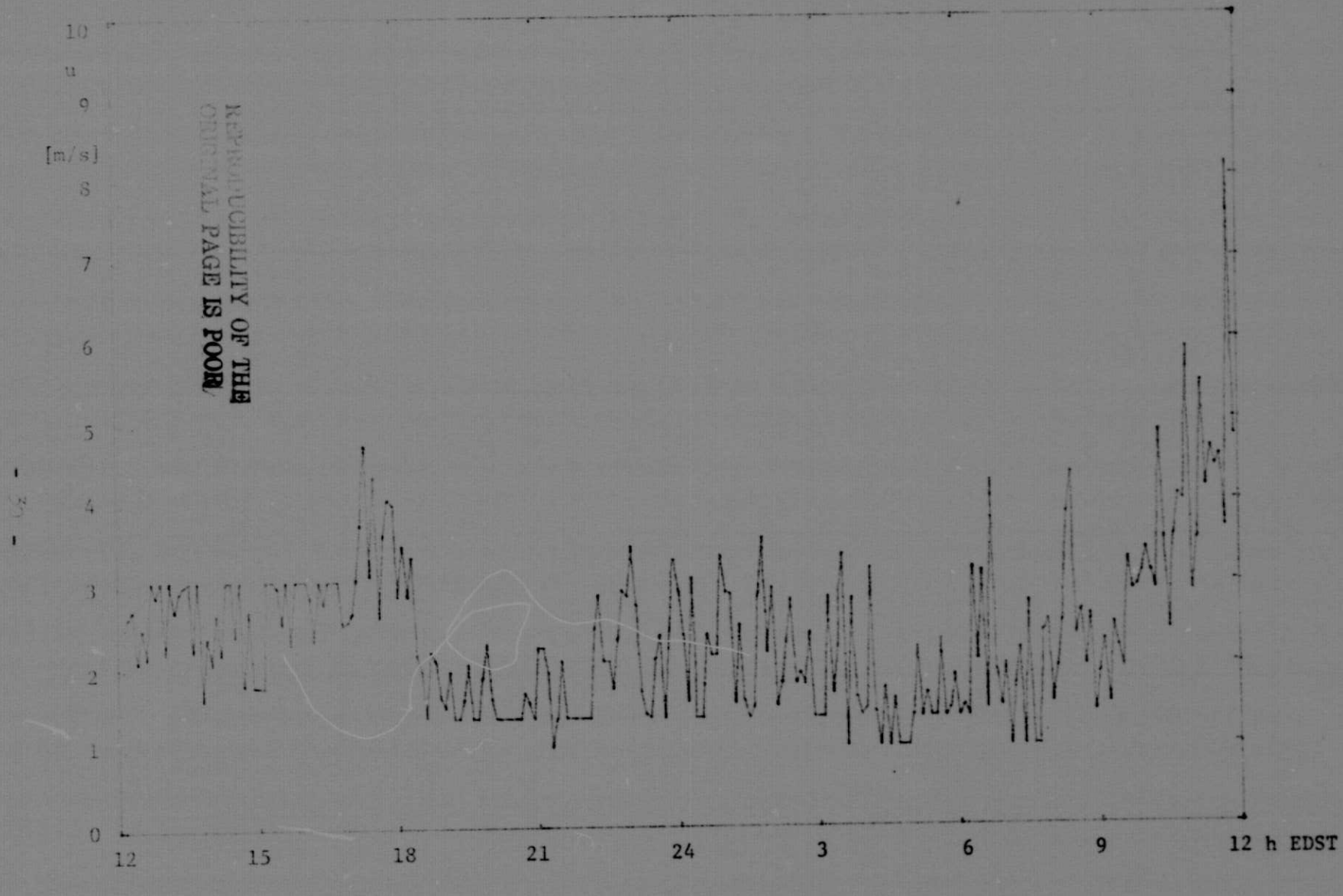

Figure 17. Wind speed at 150 cm on October 13/14.

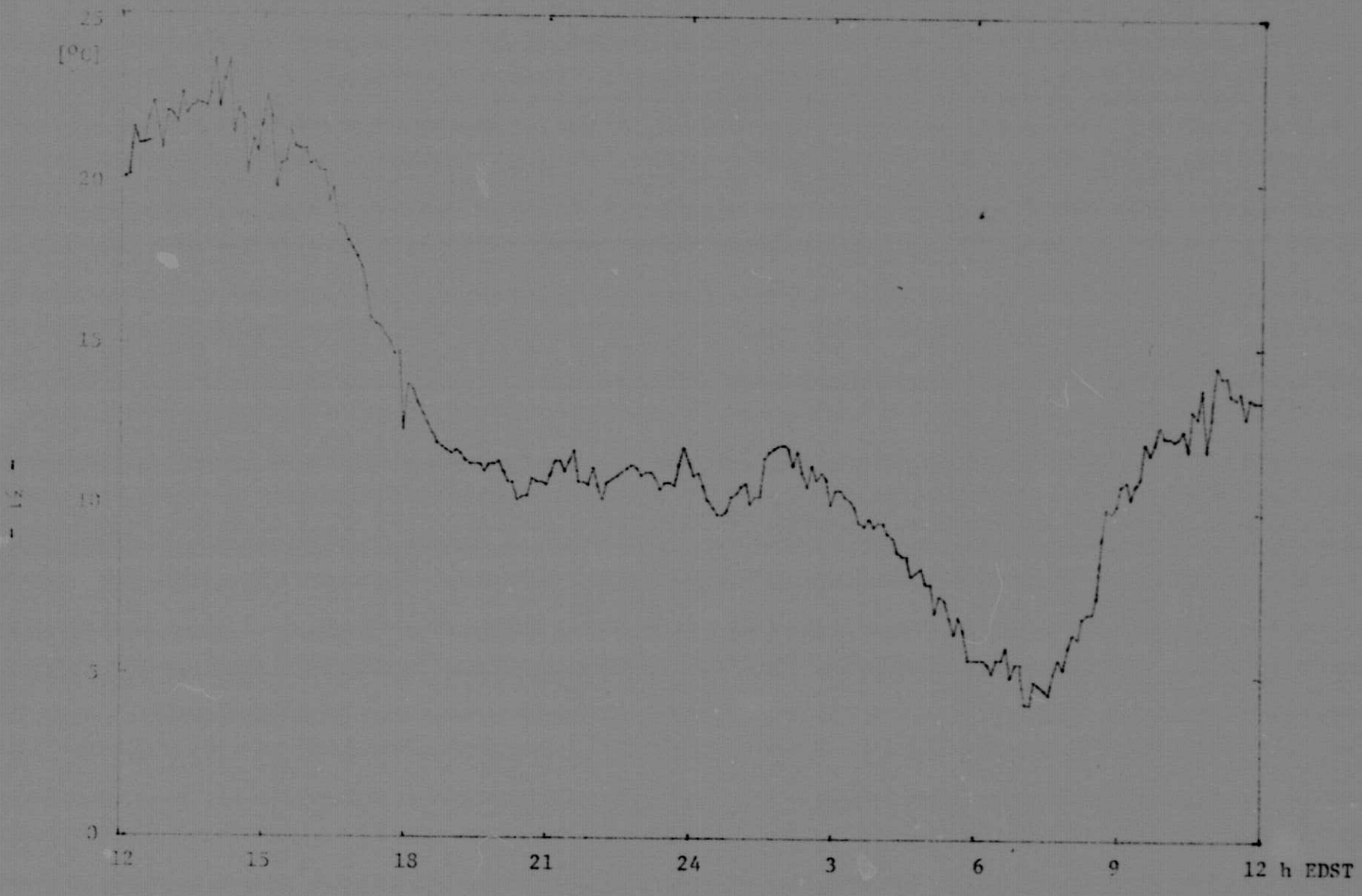

Figure 18. Air temperature at 10 cm on October 13/14.

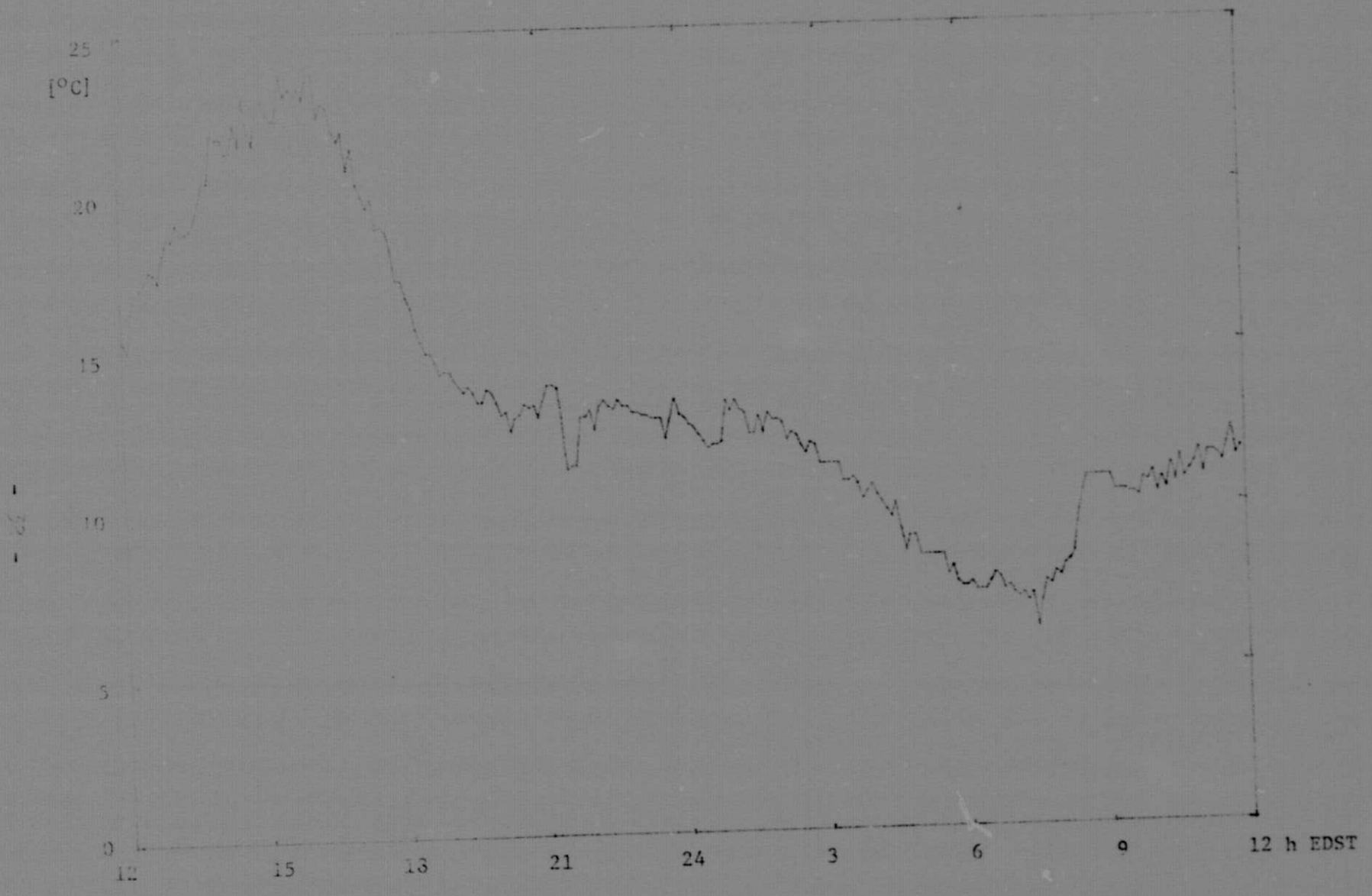

Figure 19. Air temperature at 150 cm on October 13/14.

$$E = -\frac{R_{total} + S}{1 + \gamma \frac{T_a - T_s}{e_s(T_a) - e_s(T_s)}} = 2.7 \text{ mm/d.} \qquad (36)$$

4.3 Remote Sensing Approach

According to Idso and Jackson (1975c), the 24-hour total of evaporation from a wet soil is

$$\rho LE = R_v(1-a) + 1.56\left[\sigma T_a^4\left(1-0.261\, e^{-0.000777(T_a-273)^2}\right) - \sigma T_s^4\right] + 156 \qquad (37)$$

where all energies are in cal/cm^2.

Using again daily averages of R_v, a, T_a, and T_s we obtain

$$E = 4.2 \text{ mm/d.}$$

It should be noticed that this approach does not involve a knowledge of wind speed or humidity, whereas all other approaches discussed before require knowledge of both parameters.

4.4 Soil Moisture Approach

The soil moisture at 2 cm and 5 cm is shown in Figures 20 and 21. The total change of soil moisture at 2 cm during the 24-hour period is 0.16 cm^3 H_2O per cm^3 soil. This gives only a lower limit of evaporated water of 1.6 mm/d.

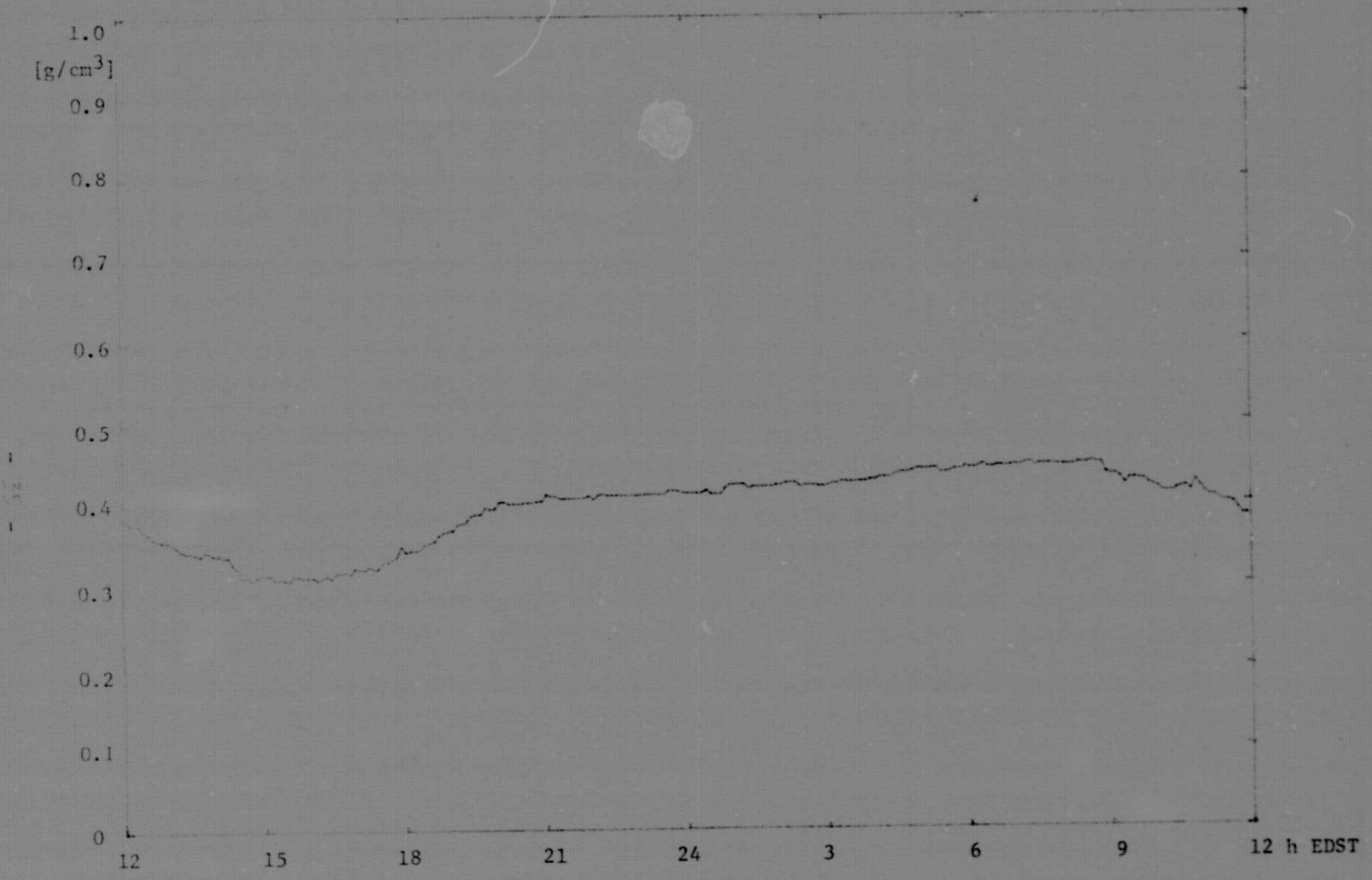

Figure 21. Soil moisture content at 5 cm on October 13/14.

5. Conclusions and Recommendations

The estimates of daily evaporation rates from all approaches agree to within 50 percent. Remote measurement of evaporation rates from bare wet soil appears feasible, even under a light cloud cover, if no better accuracy is required.

In order to improve the accuracy of evaporation estimates, the following research is recommended:

The evaporated mass of water should be monitored quantitatively using a weighing lysimeter, so that the accuracy of each individual method can be given.

The correlation between cloud cover and thermal sky radiation should be investigated quantitatively and systematically using a radiometer which is sensitive in the entire range of wavelengths from 3 to 20 μm.

Valid general procedures can only be based on a large number of observations at various conditions. In an approach to reduce the large number of variables affecting evaporation rates, certain recurring weather patterns, their frequencies and characteristics should be identified, and one should search for possible accumulations of such patterns at various times in the annual cycle and at various locations in the US.

References

Carlslaw, H. S., and J. C. Jaeger, Conduction of heat in solids, Oxford University Press, 1959, 31.

Idso, S. B., and R. D. Jackson, Thermal Radiation from the Atmosphere, J. Geophys. Res., 74, 1969, 5397-5403.

Idso, S. B., R. D. Jackson, and R. J. Reginato, Detection of soil moisture by remote surveillance, Amer. Sci., 63, 1975a, 549-557.

Idso, S. B., T. J. Schmugge, R.D. Jackson, and R.J. Reginato, The utility of surface temperature measurements for the remote sensing of soil water status, J. Geophys. Res., 80, 1975b, 3044-3049.

Idso, S. B., R. D. Jackson, and R.J. Reginato, Estimating Evaporation: A technique adaptable to remote sensing, Science, 189, 1975c, 991-992.

Penman, H. L., Natural evaporation from open water, bare soil and grass, Proc. Royal Soc. London, 193 ser.A, 1948, 120-145.

Rohwer, C., US Dept. Agric. Tech. Bull. 271, 1931.